Journal of Power Sources 209 (2012) 243–250

Contents lists available at SciVerse ScienceDirect

Journal of Power Sources

journal homepage: www.elsevier.com/locate/jpowsour

Electrochemical capacitive behaviors of ordered mesoporous carbons with controllable pore sizes

Hongling Lu[a,1], Weijie Dai[a,1], Mingbo Zheng[b], Nianwu Li[a], Guangbin Ji[a], Jieming Cao[a,*]

[a] Nanomaterials Research Institute, College of Materials Science and Technology, Nanjing University of Aeronautics and Astronautics, Nanjing 210016, China
[b] National Laboratory of Microstructures, School of Electronic Science and Engineering, Nanjing University, Nanjing 210093, China

ARTICLE INFO

Article history:
Received 29 November 2011
Received in revised form 9 February 2012
Accepted 13 February 2012
Available online 22 February 2012

Keywords:
Electrochemical double layer capacitors
Ordered mesoporous carbons
Pore size control
Template synthesis

ABSTRACT

Ordered mesoporous carbons (OMCs) with controllable pore sizes in the range of 4–10 nm are prepared by a template procedure using 2D hexagonal MSU-H and 3D cubic KIT-6 as hard templates and boric acid as the pore expanding agent. The electrochemical performances of the as-synthesized OMCs as electrode materials for electrochemical double layer capacitors (EDLCs) are characterized by cyclic voltammetry (CV), galvanostatic charge/discharge (GC) and electrochemical impedance spectroscopy (EIS) experiments in 30 wt% KOH electrolyte. The influence of the pore size distributions of OMCs on the electrochemical capacitive performances is discussed. The prepared OMCs exhibit good capacitive behaviors with the specific capacitance values ranging from 143 to 205.3 F g^{-1} at a voltage scan rate of 5 mV s^{-1} and 81 to 86% retained at a high scan rate of 100 mV s^{-1}. OMC-M-2 shows the highest specific surface capacitance value of 27.5 μF cm^{-2} at 5 mV s^{-1} with a peak pore size of 7.8 nm and a Brunauer–Emmet–Teller (BET) surface area of 729.3 m^2 g^{-1}. The analysis of two kinds of pore symmetries of OMCs with the same pore size of about 6.5 nm shows that the 3D cubic OMC exhibited superior capacitive performance than the 2D hexagonal OMC.

1. Introduction

Over the last decade, OMCs have been studied widely in many fields such as adsorbents, catalysts, gas storage, and biosensors due to their narrow pore size distributions, high surface areas and high pore volumes [1–5]. Recently, many researches have demonstrated that OMCs have promising electrochemical capacitive properties in the application of EDLCs [6–9]. EDLCs utilize the electric double layer formed at the electrode/electrolyte interface where charges are accumulated on the electrode surfaces and ions of opposite charge compensate them. On the basis of this mechanism, the electrode material should have a high surface area for charge accumulation. Activated carbons with high surface area are currently used as the electrode materials for EDLCs due to their low cost and a wide variety of carbon precursors. However, activated carbons that only contain micropores (<2 nm) have no interconnected porous network with sufficient open pore windows for electrolyte wetting and rapid ionic transport. Moreover, even if the micropores are wetted by the electrolyte, the ionic motion is still restricted in such small pores, inducing the high rate capability unrealised. Considering the above limitations, ordered mesoporous carbons with regularly interconnected mesopores (2–50 nm) are desired for EDLCs electrodes owning to that the ordered mesoporous channels and a noticeable volume of micropores can provide a large surface area for dispersion of the active sites [10–14]. Thus, OMCs should have better electrochemical capacitive properties than conventional activated carbons at high current densities. Xing et al. [15] prepared a series of highly OMCs with 3D cubic and 2D hexagonal spacer group, the results indicated that there are different electrochemical capacitive properties between the two kinds of materials with different pore structures, and OMC-3D demonstrated excellent high-frequency performances due to its higher surface area in pores larger than 3 nm. Unfortunately, the capacitive performance of conventional OMCs is still not satisfying owning to the low surface capacitance. Generally speaking, the surface capacitance of OMC can achieve 20 μF cm^{-2} [8], but it is only about 8–10 μF cm^{-2} according to the reported literatures [16–18]. Therefore, systemic research into the effect of pore structure of OMCs on the electrochemical capacitive performance is required to optimize the capability of the OMCs. Herein, OMCs with controllable pore size distribution and different pore symmetries were synthesized by the template method and the influence of pore structure on the capacitive behaviors was discussed in detail.

The template carbonization method is very attractive to synthesize the OMC materials for the reason that the carbon structure

* Corresponding author at: College of Materials Science and Technology, Nanjing University of Aeronautics and Astronautics, Nanjing, Jiangsu Province 210016, China. Tel.: +86 25 84895289; fax: +86 25 84895289.
E-mail address: jmcao@nuaa.edu.cn (J. Cao).
[1] These authors contributed equally to this work.

0378-7753/$ – see front matter © 2012 Elsevier B.V. All rights reserved.
doi:10.1016/j.jpowsour.2012.02.041

in terms of various aspects, such as pore structure and microscopic morphology, is easily controllable. Since the first synthesis of ordered mesoporous carbon, denoted as CMK-1, was reported by Ryoo et al. using the MCM-48 silica with cubic Ia3d symmetry as the template [19], many kinds of OMC materials with different structures have been prepared using various types of silica templates [20–24]. Recently, Lee et al. reported the synthesis of OMC materials with tunable mesopore sizes in the range of 3–10 nm employing boric acid as the pore expanding agent [25]. According to the pore expansion mechanism, the boric acid was mixed with the carbon precursor firstly, and then the boron species spontaneously separated from the mixture of boron and carbon precursors to the silica surface of mesoporous silica template during the carbonization process. Subsequently, the boron oxide and borosilicate nanolayers were formed between the silica and carbon frameworks. By removal of the silica and the boron layer using HF solution, the OMC materials with an increased pore size was obtained finally. A 2D hexagonal mesoporous silica, MSU-H, was used as the silica template in their previous report [26].

In the present work, we synthesized two kinds of OMC materials with controllable pore sizes using the aforementioned 2D hexagonal MSU-H and cubic KIT-6 (Ia3d), which contains 3D bicontinuous channel networks, as hard templates. The sucrose was used as the carbon precursor and the boric acid as an agent aiming to expand the pore sizes gradually by controlling the amount of the boric acid during the process of carbonization. The prepared OMC materials were studied as electrode materials for supercapacitor applications and the relationship between the pore structures and electrochemical capacitive properties of the carbon materials was investigated.

2. Experimental

2.1. Synthesis of MSU-H silica

The 2D hexagonal mesoporous silica MSU-H was synthesized at near-neutral pH conditions using a low cost sodium silicate as the silica precursor and Pluronic P123 ($EO_{20}PO_{70}EO_{20}$, MW = 5800, Sigma–Aldrich) as a structure-directing agent. In a typical synthesis, 6 g of Ludox-HS40 (Sigma–Aldrich) was mixed with 10 mL of NaOH aqueous solution (10 mol L^{-1}) at 80 °C. After complete dissolution, the sodium silicate solution was cooled down to the room temperature and then added to 152 mL of P123 aqueous solution (0.11 mol L^{-1}) at 25 °C. After stirring for 10 min, 6 g of acetic acid was added to the mixture for neutralization (pH ~ 7.0). Followed by stirring for 10 min, the mixture was heated to 45 °C and further left stirring for 24 h. And then the mixture was transferred into a Teflon-lined stainless steel autoclave and maintained at 100 °C for 24 h under static conditions in an oven. The solid product was filtered, washed, air-dried and subsequently calcined in air at 550 °C for 6 h.

2.2. Synthesis of KIT-6 silica

The cubic Ia3d mesoporous silica KIT-6 was prepared following the method reported by Kleitz et al. [21] with slight modifications. Briefly, 5 g of Pluronic P123 was dissolved in 153.8 g of distilled water and 10 g of HCl (37 wt%) under vigorous stirring at 35 °C. After complete dissolution, 5 g of butanol was added. Following further stirring for 1 h, 10.75 g of TEOS was added immediately. Subsequently, the mixture was left stirring at 35 °C for 24 h and transferred into an autoclave which was sealed and maintained at 100 °C for another 24 h under static conditions. The resulting solid product was filtered and dried at 100 °C overnight. After a brief ethanol/HCl washing, the final sample was dried at 70 °C and calcined at 550 °C for 6 h in air.

2.3. Synthesis of ordered mesoporous carbons

The synthesis of OMCs with tunable pore sizes was performed using the mixture of sucrose and boric acid as the precursor solutions which were prepared by adding various amount of boric acid to the sucrose solution while keeping the sucrose concentration constant. The mesoporous carbon replicas of the MSU-H and KIT-6 silica templates were designated as OMC-M-*x* and OMC-K-*y*, respectively, where *x* and *y* stand for the molar ratio of boric acid to sucrose. A typical preparation of OMC-M-2 was as follows: 0.226 g of boric acid, 0.625 g of sucrose and 0.071 g sulfuric acid were dissolved in 2.5 g of distilled water. After 0.5 g of MSU-H silica was added, the mixture was heated at 100 °C for 6 h, and subsequently 160 °C for another 6 h. The resulted composite was impregnated again with an aqueous solution consisting of 0.15 g of boric acid, 0.413 g of sucrose, 0.047 g of sulfuric acid and 2.5 g of distilled water. After retreated at 100 °C and 160 °C as before, the composite was carbonized at 900 °C for 3 h under N_2 flow. The silica template was removed using 5 wt% HF solution at the room temperature and the OMC-M-2 material was obtained finally. The OMC-K materials were synthesized by the same method using KIT-6 instead of MSU-H as the silica template.

2.4. Porosity measurement

The porous structure parameters of all the samples were determined from N_2 adsorption–desorption isotherms which were measured on a Micromeritics ASAP 2010 system at the liquid nitrogen temperature with prior degassing of all the samples under vacuum at 200 °C. The surface area was calculated by the BET method. The micropore surface area was estimated using the *t*-plot method. The pore size distribution was analyzed with the adsorption branch using the Barrett–Joyner–Halenda (BJH) algorithm. The total pore volume was calculated from the amount adsorbed at a relative pressure of 0.99. Transmission electron microscopy (TEM) images were taken on a JEOL (JEM-200CX) microscope at an accelerating voltage of 200 kV.

2.5. Electrochemical characterization

The electrodes were prepared by mixing 80 wt% of OMC sample, 15 wt% of acetylene black and 5 wt% of PTFE binder dispersed in ethanol. The resulting slurry was rolled onto the Ni foam which was dried at 100 °C overnight and then pressed at 10 MPa to get an approximate thickness of 0.2 mm. The loading density of each electrode material was 5 mg cm^{-2}. The tests were carried out in a three-electrode arrangement using Platinum foil and saturated calomel electrode (SCE) as counter and reference electrode respectively in alkaline electrolyte of 30 wt% KOH. CV and GC were carried out on CHI660C electrochemical working station in a potential range of −1 to −0.2 V vs. SCE. EIS measurements were recorded from 20 kHz to 10 mHz with AC amplitude of 10 mV on Solartron 1287/1260 electrochemical system.

3. Results and discussion

3.1. Structural and adsorption properties

The TEM images of OMC-M-0 and OMC-K-4 are shown in Fig. 1. It reveals that the carbon materials exhibit ordered mesoporous structures, indicative of excellent replication of the mesoporous template silica MSU-H and KIT-6.

Table 1
Textural properties of mesoporous silica templates and OMC materials.

Samples	d_0 (nm)	S_{BET} ($m^2\,g^{-1}$)	S_{micro} ($m^2\,g^{-1}$)	V_{tot} ($cm^3\,g^{-1}$)	V_{micro} ($cm^3\,g^{-1}$)
MSU-H	12.5	318.8	24.9	1.04	–
OMC-M-0	4.3	964.6	329.5	1.22	0.16
OMC-M-1	6.4	773.2	298.3	1.15	0.14
OMC-M-2	7.8	729.3	311.8	1.11	0.15
OMC-M-4	8.2	699.1	258.1	1.46	0.12
OMC-M-6	8.5	868.5	376.2	1.75	0.18
KIT-6	7.5	790.2	105.4	1.11	–
OMC-K-0	3.9	1188.3	217.9	1.33	0.10
OMC-K-1	4.9	692.7	200.1	0.98	0.09
OMC-K-4	5.7	955.8	435.6	1.32	0.21
OMC-K-8	6.6	779.2	404.2	1.27	0.19
OMC-K-12	9.4	1017.9	550.5	1.68	0.27

d_0, the peak pore diameter calculated using the BJH method from the adsorption branch of the isotherm; S_{BET}, specific surface area; S_{micro}, micropore surface area; V_{tot}, total pore volume; V_{micro}, micropore volume.

Nitrogen adsorption–desorption isotherms and corresponding pore size distributions for the prepared mesoporous silica templates and carbon replicas are shown in Fig. 2. The sorption isotherms for all samples represent type IV isotherm with an obvious capillary condensation step which reflects the mesoporous structure. As for the carbon replicas, the shift of the capillary condensation step to higher relative pressure with increasing boron content indicates the increase of the mespore size, which is confirmed by the pore size distributions showed in Fig. 2C and D. Therefore, we confirm that the pores of OMC materials can be expanded gradually by increasing the amount of boric acid in the carbon precursor, regardless of the pore symmetry of the template silica. Moreover, the pore sizes of OMC-K materials are more narrowly distributed than those of OMC-M materials although the OMCs derived from high boron content have broader pore size distributions (Fig. 2C and D). The textural properties of all samples are summarized in Table 1. In the case of OMC-K-12, the median pore diameter reaches to 9.4 nm, which is larger than that of KIT-6 silica template. It means that, compared with the pore size of OMC-M materials, the pore size of OMC-K materials can be expanded larger than that of the original silica template. Although the boron content used for preparing the OMC-M materials is lower than that for OMC-K materials, the above result may be ascribed to the different mesoporous structures of silica templates, which can be inferred from the geometrical calculation.

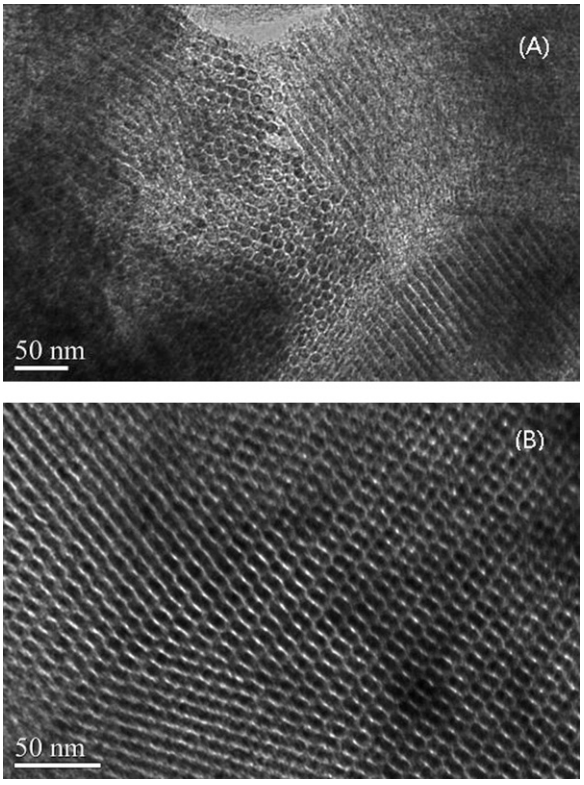

Fig. 1. TEM images of (A) OMC-M-0 and (B) OMC-K-4.

3.2. Electrochemical properties

The cyclic voltammograms of the prepared OMC electrodes in 30 wt% KOH aqueous electrolyte are presented in Fig. 3. The nearly rectangular shape at voltage scan rate of $5\,mV\,s^{-1}$ observed in Fig. 3A and B for OMC-M and OMC-K samples, respectively, indicates good electrochemical double layer capacitive behaviors. Besides, the cyclic voltammograms of OMC-M-2 and OMC-K-1 with different voltage scan rates from $5\,mV\,s^{-1}$ to $100\,mV\,s^{-1}$ are shown in Fig. 3C and D, respectively. It is noteworthy that the CV curves maintain regular box-like shape characteristics in high voltage scan rates, which is indicative of excellent quick charge propagation. The specific capacitance values of all OMCs listed in Table 2 are calculated by the formula $C_m = (1/(2 \cdot \Delta V \cdot m)) \int_{V_{initial}}^{V_{final}} (|i|/(dV/dt))dV$ [27], where $V_{initial/final}$ is the starting/end potential in one cycle, $|i|$ is the instantaneous current at a given potential, dV/dt is the potential sweep rate, m is the mass of active material in the electrode, and ΔV is the potential window. It is noticeable that the specific capacitances of OMCs increase variously after their pores were expanded. The maximum specific capacitances of up to $205.3\,F\,g^{-1}$ and $190.4\,F\,g^{-1}$ are obtained at voltage scan rate of $5\,mV\,s^{-1}$ for OMC-M-6 and OMC-K-4, respectively.

To evaluate the electrolyte ion transport efficiency, the relationship between the capacitance retention ratio and the voltage scan rate is plotted in Fig. 4A and B. It is obvious that the retention ratios of the prepared OMCs range from 81% to 86% at the high voltage scan rate of $100\,mV\,s^{-1}$, which is much higher than results reported for other OMCs [28] and means the two kinds of OMC materials with pore sizes in the range of 4–10 nm exhibit great ion transport behavior. The OMCs with comparatively larger pore sizes, e.g. OMC-M-4 and OMC-K-8, retain higher capacitance retention ratios indicating the faster electrolyte ion diffusion in such mesopore sizes, which is probably attributed to that the large mesopores and interconnected mesoporous channels of OMC-M

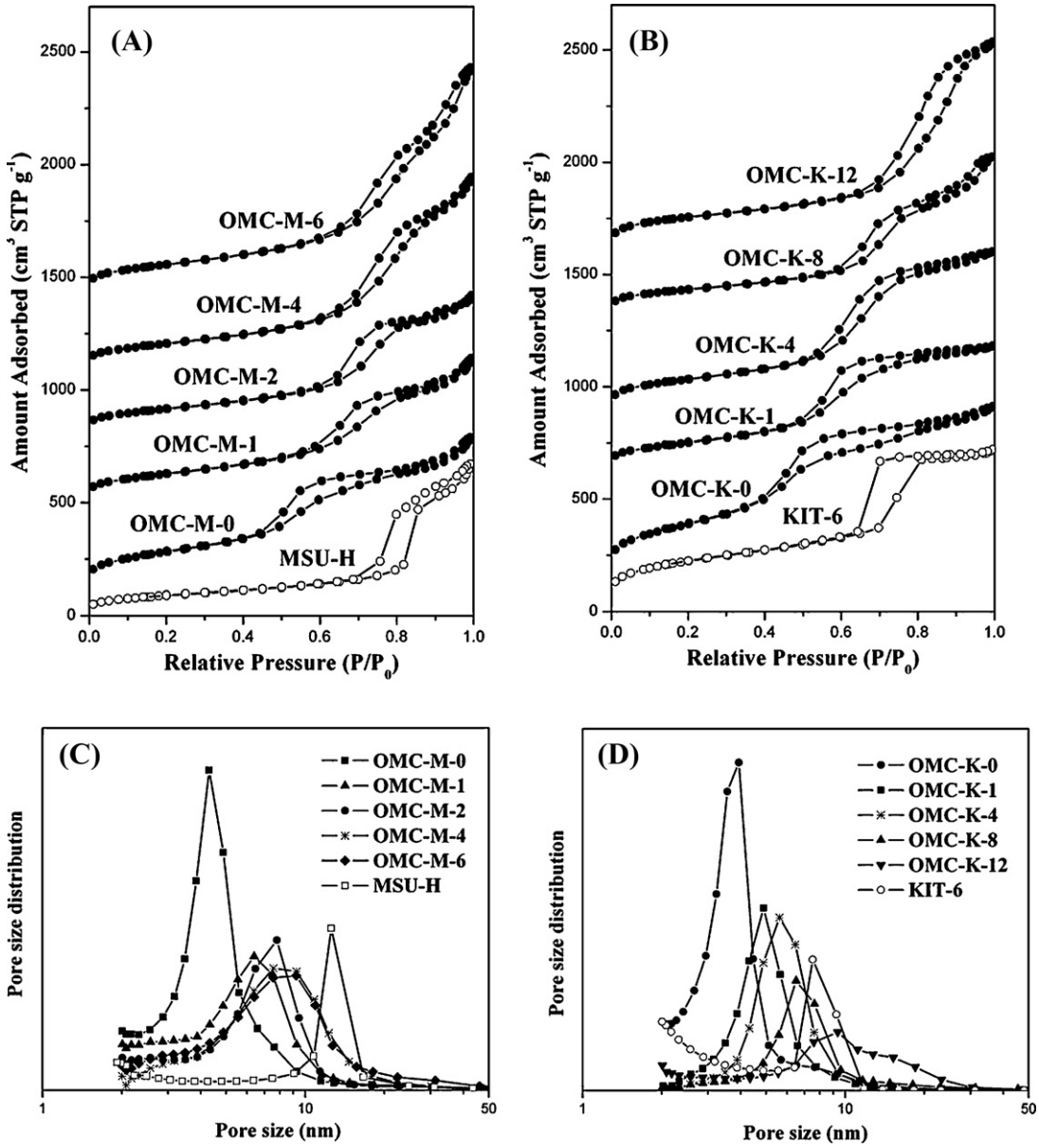

Fig. 2. (A) N_2 adsorption–desorption isotherms for MSU-H silica template and the OMC-M replicas. The sorption isotherms for the OMC-M-1, OMC-M-2, OMC-M-4 and OMC-M-6 have been shifted vertically by 400, 800, 1000 and 1300 $cm^3\ g^{-1}$, respectively. (B) N_2 adsorption–desorption isotherms for KIT-6 silica template and the OMC-K replicas. The sorption isotherms for the OMC-K-0, OMC-K-1, OMC-K-4, OMC-K-8 and OMC-K-12 have been shifted vertically by 50, 550, 750, 1200, and 1450 $cm^3\ g^{-1}$, respectively. (C) and (D) Corresponding pore size distributions for silica templates and carbon replicas calculated from adsorption branches using the BJH algorithm.

Table 2
Capacitances at different voltage scan rates for all OMC materials.

Samples	Specific capacitance at different voltage scan rates ($F\ g^{-1}$)					Specific surface capacitance at 5 mV s^{-1} ($\mu F\ cm^{-2}$)
	5 mV s^{-1}	10 mV s^{-1}	20 mV s^{-1}	50 mV s^{-1}	100 mV s^{-1}	
OMC-M-0	162.2	158.8	151.9	143.3	132.8	16.8
OMC-M-1	166.9	163.0	158.2	149.8	139.5	21.6
OMC-M-2	200.7	195.9	189.7	178.7	165.6	27.5
OMC-M-4	171.4	168.1	162.7	154.4	144.4	24.5
OMC-M-6	205.3	198.8	191.1	179.2	166.2	23.6
OMC-K-0	143.0	138.1	132.0	124.4	116.7	12.0
OMC-K-1	156.0	151.6	145.7	139.1	132.7	22.5
OMC-K-4	190.4	184.8	178.1	168.3	157.3	19.9
OMC-K-8	170.2	165.9	160.4	153.7	146.4	21.8
OMC-K-12	167.2	162.9	156.7	148.3	138.6	16.4

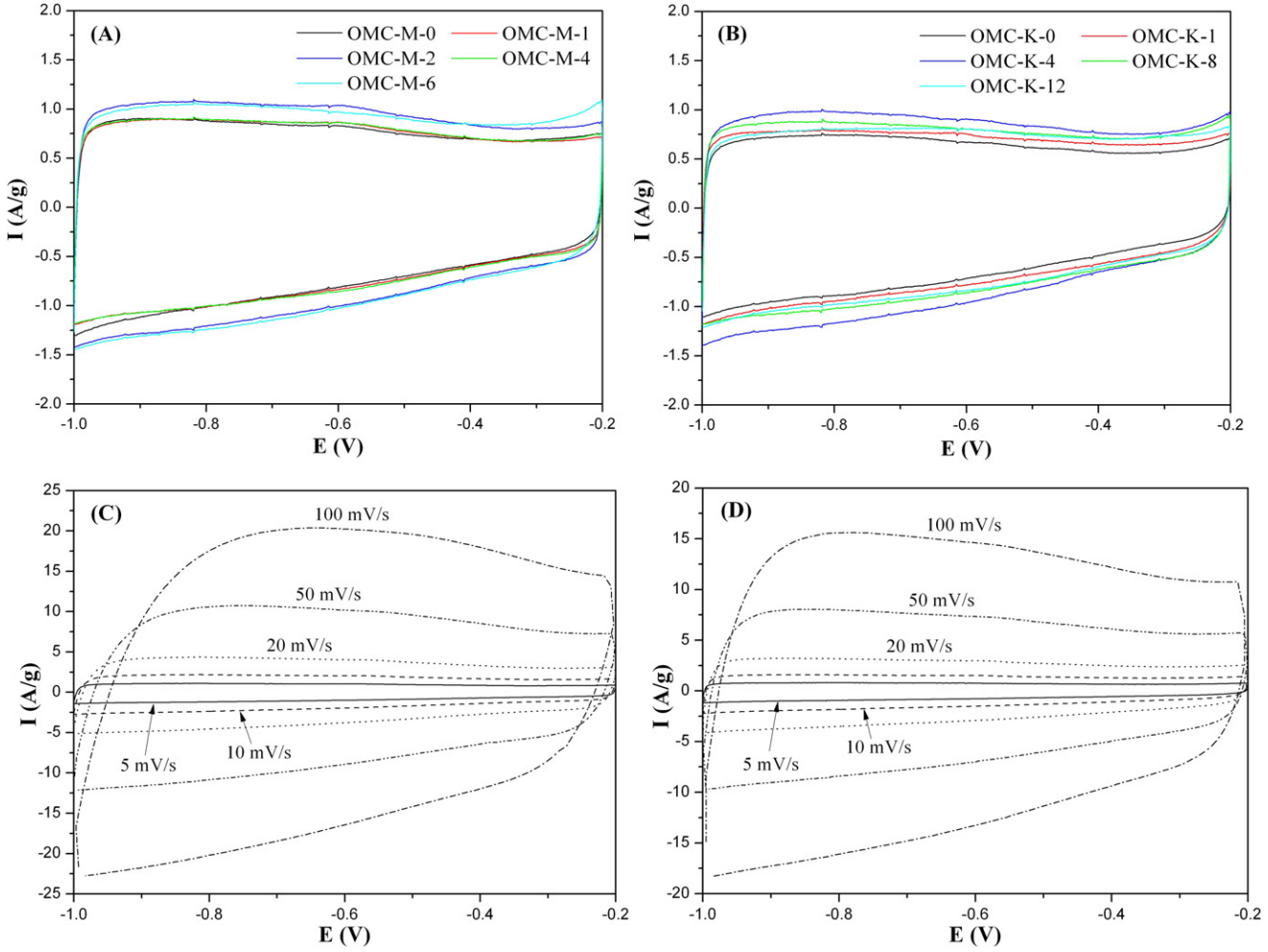

Fig. 3. Cyclic voltammograms of (A) OMC-M and (B) OMC-K electrodes at voltage scan rate of 5 mV s^{-1}, as well as (C) OMC-M-2 and (D) OMC-K-1 electrodes at different voltage scan rates in 30 wt% KOH.

and OMC-K materials reduce the resistance of ionic diffusion and facilitate the accessibility of the ions to the electrochemical active surface.

The relationship between the pore size and the capacitance retention ratio of C_{100} to C_5, where C_{100} and C_5 stand for specific capacitances at voltage scan rate of 100 mV s^{-1} and 5 mV s^{-1}, respectively, is plotted in Fig. 4C. It is notable that the OMC-K materials exhibit slightly higher capacitance retention ratios than OMC-M materials in the pore size range of 4–10 nm. Interestingly, some literatures have demonstrated that the 3D cubic mesoporous carbons with pore sizes smaller than 3 nm exhibit inferior capacitive performance than 2D hexagonal mesoporous carbons [15,28]. Thus, we further believe that the pores of OMCs larger than 4 nm play an important role in improving the capacitive performance for EDLCs.

Besides, the relationship of the specific surface capacitance (capacitance per specific surface area) with the pore size is investigated and illustrated in Fig. 4C. The specific surface capacitance at the voltage scan rate of 5 mV s^{-1} substantially increases with the enlargement of the pore sizes. The highest specific surface capacitance reaches to 27.5 μF cm^{-2} for OMC-M-2 with a peak pore size of 7.8 nm and a BET surface area of 729.3 m^2 g^{-1}, whereas the values of OMC-M with pore sizes larger than 8 nm decline slowly, which may be a consequence of structural breakdown existed in these OMC materials [25]. This analogous phenomenon can be observed in the OMC-K materials with the exception of OMC-K-1.

To further understand the influence of the mesopore structure of OMCs on the electrochemical double layer capacitive behavior, two kinds of OMCs with almost the same mesopore size and BET surface area, OMC-M-1 (6.4 nm, 773.2 m^2 g^{-1}, respectively) and OMC-K-8 (6.6 nm, 779.2 m^2 g^{-1}, respectively), are investigated and their voltammograms are showed in Fig. 5 with different voltage scan rates from 10 to 100 mV s^{-1}. It is obvious that the rectangular shape of voltammograms for OMC-K-8 exhibits lower distortion than that of OMC-M-1 with the increase of voltage scan rate, which correlates with the higher capacitance retention ratio of 86% for OMC-K-8 than that of 83.6% for OMC-M-1. Moreover, OMC-K-8 possesses a specific surface capacitance of 21.8 μF cm^{-2} at the voltage scan rate of 5 mV s^{-1}, a little larger than that of OMC-M-1 (21.6 μF cm^{-2}). The superior capacitive behaviors of OMCs with 3D cubic structure are presented when the mesopores are large enough to facilitate ion transport by providing smaller resistance and shorter diffusion pathways [29–32].

In addition, galvanostatic charge/discharge curves of the prepared OMC electrodes at current density of 1 A g^{-1} in 30 wt% KOH aqueous solution are shown in Fig. 6. The charge curves are almost linear and mirror symmetrical to their discharge

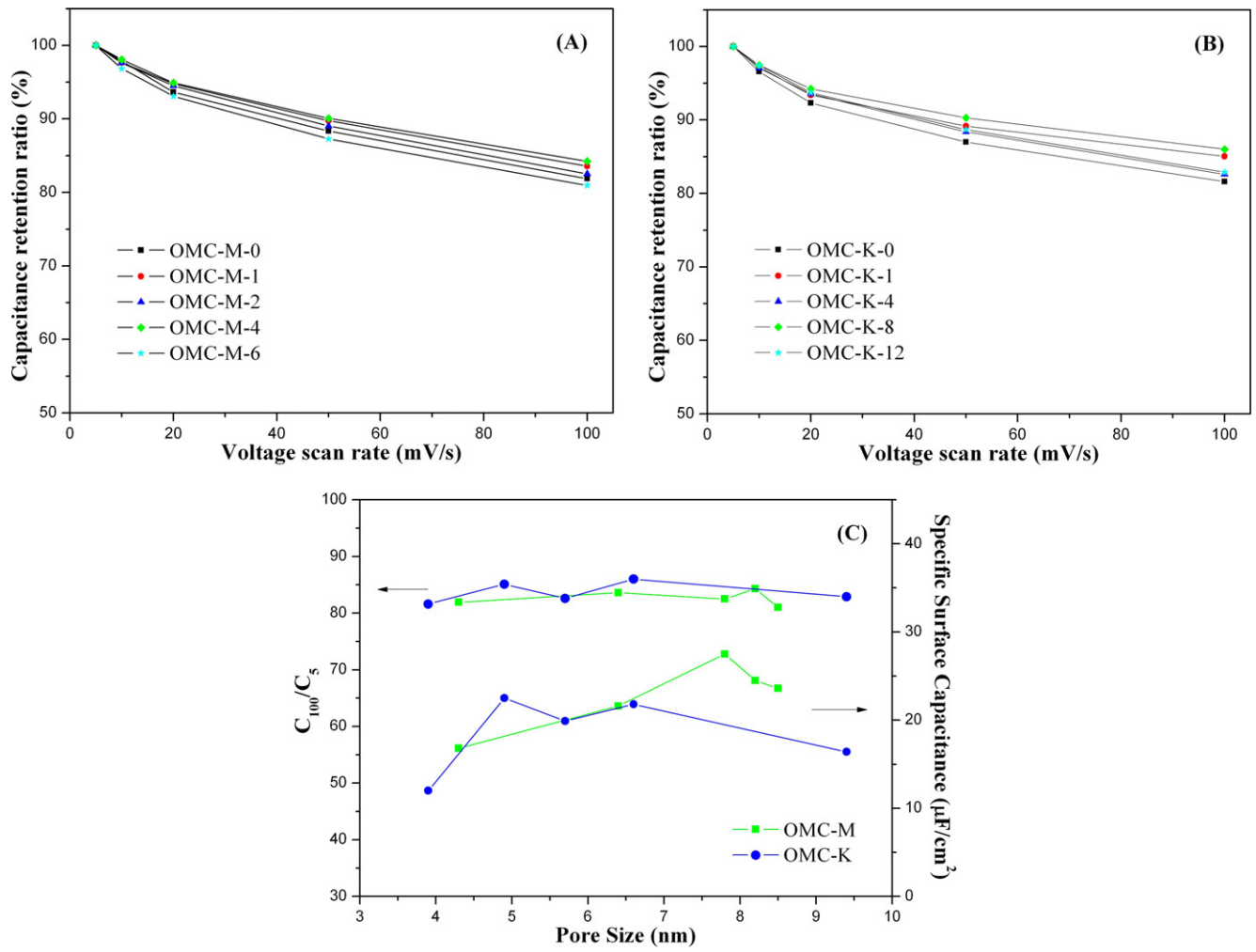

Fig. 4. The capacitance retention ratio change of (A) OMC-M and (B) OMC-K electrodes with voltage scan rates; (C) the changes of the specific surface capacitance and C_{100}/C_5 with the pore sizes.

counterparts, which is indicative of great electrochemical double layer capacitive performance. An extremely small voltage drop at the beginning of the discharge is observed for all carbon samples, which is associated with the low equivalent series resistance (ESR) of supercapacitors [33,34]. The specific capacitances of the electrodes can be calculated by $C = I \times \Delta t/(\Delta V \times m)$, where C is the specific capacitance, I is the constant discharge current, Δt is the discharge time, ΔV is the potential drop during discharge, and m is the mass of OMC material in the electrode. The obtained specific capacitances at various current densities for all carbon samples are listed in Table 3, which are in agreement with the capacitance values calculated from CV curves.

Electrochemical impedance spectroscopy (EIS) which is considered to be a powerful technique for obtaining the dynamic ion

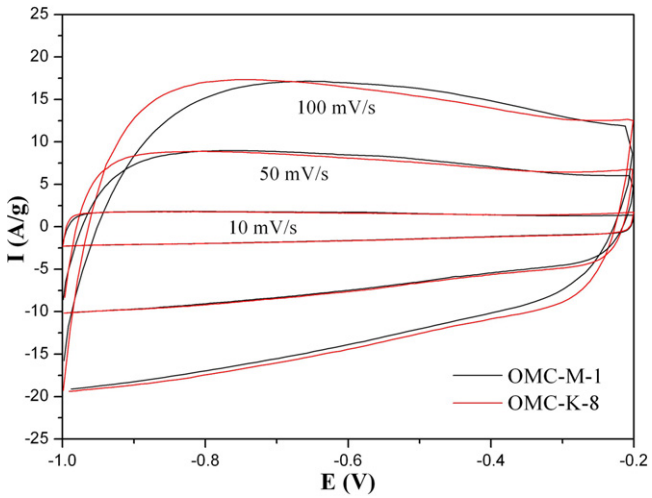

Fig. 5. Cyclic voltammograms of OMC-M-1 and OMC-K-8 at different voltage scan rates in 30 wt% KOH.

Table 3
Specific capacitances at different current densities for all OMC samples.

Samples	Specific capacitance at different current densities ($F g^{-1}$)			
	$1 A g^{-1}$	$2 A g^{-1}$	$4 A g^{-1}$	$10 A g^{-1}$
OMC-M-0	159.3	152.5	146.1	134.9
OMC-M-1	159.9	155.4	149.3	139.4
OMC-M-2	193.4	186.4	179.5	168.3
OMC-M-4	161.8	156.4	150.8	142.8
OMC-M-6	202.8	192.8	184.0	172.5
OMC-K-0	136.6	130.3	124.0	116.3
OMC-K-1	149.5	143.5	138.0	130.1
OMC-K-4	185.3	176.4	170.3	159.8
OMC-K-8	165.8	159.6	153.7	146.3
OMC-K-12	160.8	153.5	146.7	136.1

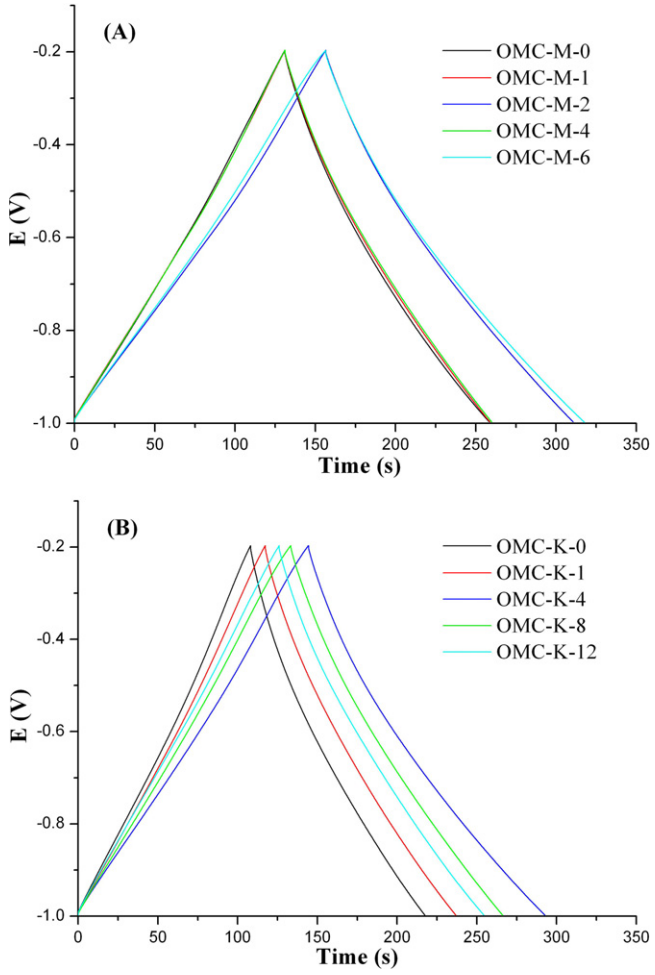

Fig. 6. Galvanostatic charge/discharge curves of (A) OMC-M and (B) OMC-K electrodes at current density of 1 A g^{-1} in 30 wt% KOH aqueous solution.

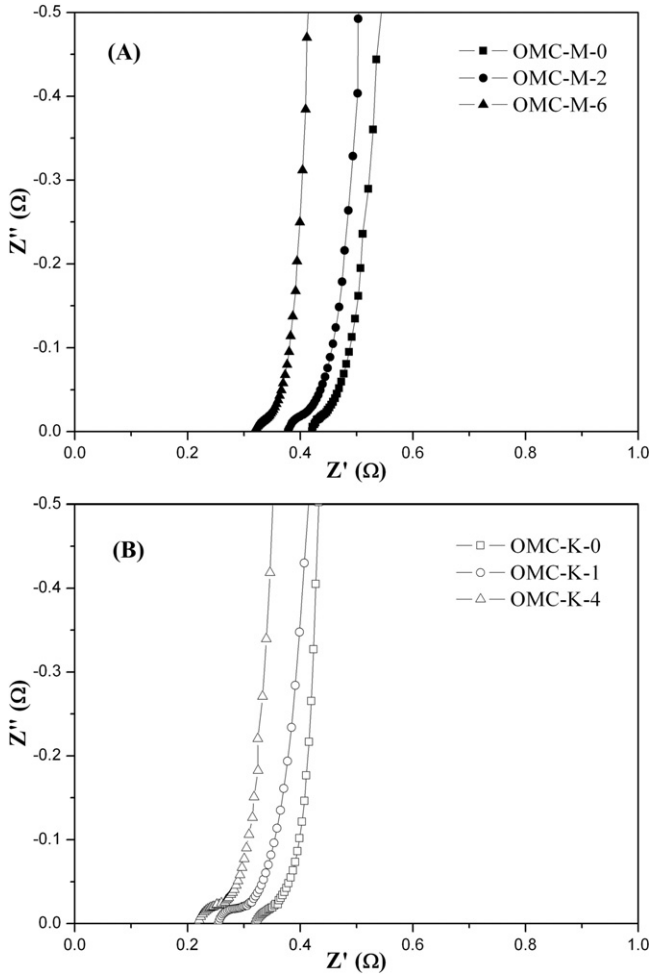

Fig. 7. Nyquist plots for different carbon electrodes in 30 wt% KOH: (A) OMC-M-0, OMC-M-2, and OMC-M-6; (B) OMC-K-0, OMC-K-1, and OMC-K-4.

diffusion information [35] is further employed to analyze the influence of pore structure on electrochemical property. The Nyquist plots for all carbon electrodes in 30 wt% KOH are given in Fig. 7. The plots for all samples are characterized by a semicircle at high frequency, a linear part with an angle of 45° in medium frequency region and a straight line nearly vertical to the real impedance axis at low frequency, which is suggestive of an admirable capacitive behavior. The diameter of the semicircle is referred to as the polarization resistance R_P [36] which reflects the penetration of the electrolyte into the pores of the samples. Generally, the larger pore size, the better efficiency ion diffusion is [37]. It can be seen that the R_P values of OMC-M-2 with pore size of 7.8 nm and OMC-M-6 with pore size of 8.5 nm are smaller than that of OMC-M-0 with pore size of 4.3 nm from Fig. 7A, indicating easier ion diffusion to the electrochemical active surface in larger pores. On the other hand, although the pore size of OMC-M-6 is larger than OMC-M-2, the R_P is larger than OMC-M-2, this may be due to the distortion of the pore structure. Similarly, the R_P of OMC-K-1 is the smallest among OMC-K materials, although the R_P values of all OMC materials are small and slight different. This is confirmed by the capacitance retention ratios described in Fig. 4A and B. Moreover, the short length of the 45° lines for all OMC samples indicates the pores in this range facilitate the electrolyte accessibility [37,38].

4. Conclusion

Ordered mesoporous carbons with 2D hexagonal and 3D cubic pore symmetries were successfully synthesized and the pore sizes were adjusted gradually in the range of 4–10 nm using the boric acid as the pore expanding agent. The prepared OMCs were investigated as electrode materials for EDLCs and the electrochemical performance was characterized by CV, GC and EIS experiments in 30 wt% KOH electrolyte. The specific capacitances of OMCs are in the range of 143–205.3 F g^{-1} at the voltage scan rate of 5 mV s^{-1}, although the BET surface areas are relatively low in the range of about 700–1200 m^2 g^{-1}. OMC-K-8 maintains the highest capacitance retention ratio of up to 86% at the high voltage scan rate of 100 mV s^{-1} while other OMCs retain no less 81%. Moreover, OMC-M-2 with a peak pore size of 7.8 nm and a BET surface area of 729.3 m^2 g^{-1} exhibits the maximum specific surface capacitance value of 27.5 μF cm^{-2} at 5 mV s^{-1}. According to the analysis of the influence of pore symmetries of OMCs on the electrochemical behavior, we find that OMCs with 3D cubic pore structure show better electrochemical performance than the OMCs with 2D hexagonal pore structure. We attribute the great electrochemical behaviors to the comparatively large mesopore sizes and interconnected mesoporous channels in the as-synthesized OMCs. These results make the OMCs with large pore sizes more advantaged for electrodes in EDLCs.

Acknowledgments

This work was supported by Natural Science Foundation of Jiangsu Province (No. BK2006195, BK2010497), National Natural Science Foundation of China (No. 51172109), China Postdoctoral Science Foundation (No. 20100471296) and Postdoctoral Foundation of Jiangsu Province (No. 1001003C).

References

[1] A. Stein, Z.Y. Wang, M.A. Fierke, Adv. Mater. 21 (2009) 265–293.
[2] A. Taguchi, F. Schuth, Microporous Mesoporous Mater. 77 (2005) 1–45.
[3] C.D. Liang, Z.J. Li, S. Dai, Angew. Chem. Int. Ed. 47 (2008) 3696–3717.
[4] J. Lee, J. Kim, T. Hyeon, Adv. Mater. 18 (2006) 2073–2094.
[5] M. Sevilla, S. Alvarez, T.A. Centeno, A.B. Fuertes, F. Stoeckli, Electrochim. Acta 52 (2007) 3207–3215.
[6] J. Lee, S. Yoon, T. Hyeon, S.M. Oh, K.B. Kim, Chem. Commun. 21 (1999) 2177–2178.
[7] J. Lee, S. Yoon, S.M. Oh, C.H. Shin, T. Hyeon, Adv. Mater. 12 (2000) 359–362.
[8] H.S. Zhou, S.M. Zhu, M. Hibino, I. Honma, J. Power Sources 122 (2003) 219–223.
[9] L. Zhou, H. Li, C.Z. Yu, X.F. Zhou, J.W. Tang, Y. Meng, Y.Y. Xia, D.Y. Zhao, Carbon 44 (2006) 1601–1604.
[10] Z.Y. Yuan, B.L. Su, J. Mater. Chem. 16 (2006) 663.
[11] C. Zou, D.C. Wu, M.Z. Li, Q.C. Zeng, F. Xu, Z.Y. Huang, R.W. Fu, J. Mater. Chem. 20 (2010) 731.
[12] Q.C. Zeng, D.C. Wu, C. Zou, F. Xu, R.W. Fu, Z.H. Li, Y.R. Liang, D.S. Su, Chem. Commun. 46 (2010) 5927.
[13] Z.Y. Wang, E. Kiesel, A. Stein, J. Mater. Chem. 18 (2008) 2194.
[14] Y.H. Deng, C. Liu, T. Yu, F. Liu, F.Q. Zhang, Y. Wan, L.J. Zhang, C.C. Wang, B. Tu, P. Webley, H.T. Wang, D.Y. Zhao, Chem. Mater. 19 (2007) 3271.
[15] W. Xing, S.Z. Qiao, R.G. Ding, F. Li, G.Q. Lu, Z.F. Yan, H.M. Cheng, Carbon 44 (2006) 216–224.
[16] C. Vix-Guterl, E. Frackowiak, K. Jurewicz, M. Friebe, J. Parmentier, F. Béguin, Carbon 43 (2005) 1293–1302.
[17] A.B. Fuertes, G. Lota, T.A. Centeno, E. Frackowiak, Electrochim. Acta 50 (2005) 2799–2805.
[18] D.W. Wang, F. Li, H.T. Fang, M. Liu, G.Q. Lu, H.M. Cheng, J. Phys. Chem. B 110 (2006) 8570–8575.
[19] R. Ryoo, S.H. Joo, S.J. Jun, Phys. Chem. B 103 (1999) 7743–7746.
[20] S.S. Kim, T.R. Pauly, T. Pinnavaia, J. Chem. Commun. 17 (2000) 1661–1662.
[21] F. Kleitz, S.H. Choi, R. Ryoo, Chem. Commun. 17 (2003) 2136–2137.
[22] S. Jun, S.H. Joo, R. Ryoo, M. Kruk, M. Jaroniec, Z. Liu, T. Ohsuna, O. Terasaki, J. Am. Chem. Soc. 122 (2000) 10712–10713.
[23] L.-C. Sang, A. Vinu, M.-O. Coppens, J. Mater. Chem. 21 (2011) 7410.
[24] L. Cao, M. Kruk, Adsorption 16 (2010) 465–472.
[25] H.I. Lee, J.H. Kim, D.J. You, J.E. Lee, J.M. Kim, W.S. Ahn, C. Pak, S.H. Joo, H. Chang, D. Seung, Adv. Mater. 20 (2008) 757–762.
[26] S.H. Joo, C. Pak, D.J. You, S.-A. Lee, H.I. Lee, J.M. Kim, H. Chang, D. Seung, Electrochim. Acta 52 (2006) 1618.
[27] K.W. Nam, K.B. Kim, J. Electrochem. Soc. 149 (2002) A346.
[28] K.S. Xia, Q.M. Gao, J.H. Jiang, J.H. Jiang, J. Hu, Carbon 46 (2008) 1718–1726.
[29] D.W. Wang, F. Li, M. Liu, G.Q. Lu, H.M. Cheng, Angew. Chem. Int. Ed. 47 (2008) 373–376.
[30] J.W. Long, B. Dunn, D.R. Rolison, H.S. White, Chem. Rev. 104 (2004) 4463–4492.
[31] J.W. Lang, X.B. Yan, X.Y. Yuan, J. Yang, Q.J. Xue, J. Power Sources 196 (2011) 10472–10478.
[32] M. Oschatz, E. Kockrick, M. Rose, L. Borchardt, N. Klein, I. Senkovska, T. Freudenberg, Y. Korenblit, G. Yushin, S. Kaskel, Carbon 48 (2010) 3987–3992.
[33] A.B. Fuertes, F. Pico, J.M. Rojo, J. Power Sources 133 (2004) 329–336.
[34] S.R.S. Prabaharan, R. Vimala, Z. Zainal, J. Power Sources 161 (2006) 730–736.
[35] H.Q. Li, J.Y. Luo, X.F. Zhou, C.Z. Yu, Y.Y. Xia, J. Electrochem. Soc. 154 (2007) A731–A736.
[36] M. Toupina, D. Bélanger, I.R. Hill, D. Quinn, J. Power Sources 140 (2005) 203–210.
[37] Ch.-L. Liu, W.S. Dong, G. Cao, J.R. Song, L. Liu, Y.S. Yang, J. Electrochem. Soc. 155 (2008) F1–F7.
[38] L. Tang, L. Zhan, G.Z. Yang, J.H. Yang, Y.L. Wang, W.M. Qiao, L.C. Ling, New Carbon Mater. 26 (2011) 237–240.